Quadrupole and hexadecapole ordering in DyB2C2: Direct observation with resonant x-ray diffraction

Quadrupole and hexadecapole ordering in DyB_2C_2:
Direct observation with resonant x-ray diffraction

Yoshikazu Tanaka,[1] Toshiya Inami,[2] Stephen W. Lovesey,[1,3] Kevin S. Knight,[3] Flora Yakhou,[4] Danny Mannix,[4]
Jun Kokubun,[5] Masayuki Kanazawa,[5] Kohtaro Ishida,[5] Susumu Nanao,[6] Tetsuya Nakamura,[6] Hiroki Yamauchi,[7]
Hideya Onodera,[7] Kenji Ohoyama,[7] and Yasuo Yamaguchi[7]

[1]*Institute of Physical and Chemical Research (RIKEN), Mikazuki, Sayo, Hyogo 679-5148, Japan*
[2]*Japan Atomic Energy Research Institute (JAERI), Mikazuki, Sayo, Hyogo 679-5148, Japan*
[3]*Diamond Light Source and ISIS Facility, Rutherford Appleton Laboratory, Oxfordshire OX11 0QX, England, United Kingdom*
[4]*European Synchrotron Radiation Facility, Boîte Postale 220, 38043 Grenoble Cedex, France*
[5]*Department of Physics, Tokyo University of Science, Noda, Chiba 278-8510, Japan*
[6]*Institute of Industrial Science, The University of Tokyo, Meguro, Tokyo 153-8505, Japan*
[7]*Institute for Materials Research, Tohoku University, Sendai, Miyagi 980-8577, Japan*
(Received 10 February 2003; revised manuscript received 7 May 2003; published 29 January 2004)

Direct evidence of the spatial ordering of Dy $4f$ quadrupole and hexadecapole moments in DyB_2C_2 is demonstrated by resonant x-ray diffraction enhanced by an electric quadrupole event ($E2$ resonance) at the Dy L_{III} absorption edge. The diffraction data show that the structural phase transition at $T_Q = 24.7$ K is accompanied by a reduction in the symmetry of the Dy site to $2/m$, from $4/m$, and the spatial ordering of the time-even Dy multipoles with A_g character. Below T_Q the crystal structure is described by the space group $P4_2/mnm$ and Dy ions occupy sites ($4c$). The distortion at T_Q involves the lattice occupied by B and C ions, and it amounts to a buckling of B-C planes that are normal to the two-fold rotation axis of $2/m$. An immediately plausible model of low-energy Dy states correlates data on the specific heat, our x-ray diffraction signals, and magnetic ordering below 15.3 K which has been observed in magnetic neutron diffraction.

I. INTRODUCTION

It has long been recognized that some rare-earth and actinide compounds have phase transitions due to long-range ordering of *f*-electron multipole (quadrupole or octupole) moments. The degenerate *f* electron system in highly symmetrical crystal fields, where the orbital degree of freedom remains, is somehow lifted at low temperatures. The ordering of such multipole moments sometimes plays an important role for the physical properties; for example, URu_2Si_2 and UPd_3 has extremely small magnetic moments; CeB_6 has a complicated magnetic-field temperature phase diagram. However, *direct* observation of the ordering of multipole moments is not easy. Neutron scattering is not a suitable method because the electrostatic coupling for neutrons is very weak. In contrast, x-ray scattering by electrons is so strong that it can be an excellent probe for the observation of the multipole moment ordering.

There are two possible methods in x-ray scattering experiments for the direct observation. One is nonresonant scattering and the other is resonant scattering. Arama and Morin have shown that the conventional Thomson (nonresonant) scattering is a direct probe for the multipole moment ordering by giving the formalism of the scattering for the multipoles.[1] It has been reported that the experiment on NdMg was successful to observe the antiferroquadrupole moment ordering.[2] However, the multipole ordering phase transition may accompany the lattice distortion, according to Neumann's principle in crystallography, namely, restrictions on physical properties are imposed by spatial symmetry and, in turn, elements of symmetry can be inferred from local

properties. In the other words, once the quadrupole moment orders in crystals, the local symmetry around the *f*-electron ion of interest is driven to lower spatial order to match to the symmetry of the quadrupolar moment.

Recently, Adachi *et al.* reported the nonresonant x-ray diffraction study on DyB_2C_2.[3] They found several forbidden reflections appear below the anti-ferro-quadrupole (AFQ) ordering transition temperature, but the intensities of those reflections cannot be explained quantitatively by the quadrupole moment of the Dy ions. Additional intensity can arise from a lattice distortion caused by the AFQ ordering transition. A structural phase transition from the room temperature space-group $P4/mbm$ to space-group $P4_2/mnm$, where the intensities of the Thomson scattering from the lattice distortion and those from the quadrupolar moment can overlap at the same reflection points, has been proposed by Tanaka *et al.*[4] and it is compatible with all the available experimental data. It is rather difficult to observe the multipole moment ordering directly by Thomson scattering. However, the conventional structural analysis using single crystals in combination with maximum entropy method might be useful to separate the contributions of the lattice distortion and the multipole moment.

We employed the resonant x-ray diffraction to observe the multipole moment ordering in DyB_2C_2 *directly*. The x-ray diffraction at an absorption edge in ions, so-called resonant x-ray diffraction (RXD), provides a useful tool to investigate a variety of ordered states, such as magnetic, charge, or orbital ordering. The atomic picture of resonance is well known: an incoming photon promotes a core electron to empty intermediate states, and it returns to the same core

hole emitting a second photon of the same energy as the incoming one. The scattering length carries site-specific information on unoccupied (valence) states on and around the resonant ion. Pioneer RXD has been made on materials which have a strong anisotropic chemical bonding by Templeton and Templeton.[5] Intensity at space-group forbidden reflections is attributed to the anisotropy of the valence shell. An important feature of the RXD signal is its dependence on the azimuthal angle Ψ (the rotation of the sample around the scattering vector). Variation of the intensity with changes in Ψ provides information on anisotropy in valence states since the intensity as a function of Ψ is a constant for spatially isotropic valence states.

While information derived from resonantly enhanced diffraction is directly about valence states accessed by photo-ejected core electrons, information on other valence states might be inferred with recourse to a suitable model. Note that the intermediate states probed by the resonance should be the same as the states which directly drive the ordering. Pitfalls in this method are well illustrated in experiments on manganites.[6] Data gathered using signal enhancement by a Mn transition of $E1$ character $1s \rightarrow p$-like states have the potential to give some information on Mn $3d$ states but it is not the simple nor robust process originally proposed.[7-10]

For the example of immediate interest, DyB_2C_2, two resonant processes in the vicinity of the Dy L_{III} absorption edge have been observed.[4,11] One is the dipole transition ($E1$) from $2p$ core shell to $5d$ valence state and the other seems to be the quadrupole ($E2$) transition from $2p$ to $4f$ valence shell. The $5d$ valence state can hybridize with the outer electrons of the surrounding atoms. Hence, experiments using the dipole transition, in which we might observe the lattice distortion caused by the multipole moment ordering, are not unambiguous or a direct observation. Obviously, it is important to observe the $E2$ transition for a *direct* observation of $4f$ multipole ordering motifs.

In this paper, we report a comprehensive study of the fascinating tetragonal rare-earth compound DyB_2C_2 (dysprosium borocarbide) including direct and unambiguous evidence of the spatial ordering of Dy $4f$ quadrupole and hexadecapole moments, by looking at the $4f$ valence shell with the RXD at $E2$ transition of the Dy L_{III} absorption edge. The work includes a full discussion of contributions to diffraction signals, at space-group forbidden reflections, obtained in nonresonant and resonant scattering. Azimuthal angle scans completed in resonance conditions are analyzed in terms of $E1$ and $E2$ events. Results from the analysis infer the low energy properties of Dy ions, including the ground-state wave function.

The phase diagram of DyB_2C_2 includes a structural phase transition at $T_Q = 24.7$ K and a magnetic phase transition at $T_C = 15.3$ K. In the magnetically ordered phase, two neighboring Dy magnetic moments along the c axis are mutually perpendicular, two neighboring moments in the basal plane normal to the c axis are almost oppositely aligned, and all the Dy moments are parallel to the basal plane. Much of the interest in DyB_2C_2 has focused on the structural phase transition following a seminal investigation which proposed an antiferro-ordering of Dy quadrupoles $\langle Q_{\alpha\beta} \rangle$ in an interpreta-

tion of specific heat, magnetization, and neutron diffraction on a single crystal.[12] (Here, α and β label orthogonal Cartesian axes with the z axis chosen parallel to the crystal c axis.)

The discovery[4] that the structural phase transition reduces the symmetry to # 136 ($P4_2/mnm$), from the room temperature space-group # 127 ($P4/mbm$) gives essential information for the quadrupole moment ordering. The change in symmetry is accompanied by doubling the unit cell along the c axis, and most importantly, a reduction of the point group of the Dy ion site from $4/m$ to $2/m$. The quadrupole moment is not allowed in the local symmetry $4/m$, but in $2/m$ due to Neumann's principle. The quadrupole components $\langle Q_{xy} \rangle$ and $\langle Q_{xx} - Q_{yy} \rangle$ have the following relations according to the space-group 136. For neighboring Dy ions along the c-axis these two components are equal in magnitude and opposite in sign, and in the basal plane normal to the c axis neighboring ions along the [110]-axis have $\langle Q_{xy} \rangle$ of one sign and $\langle Q_{xx} - Q_{yy} \rangle$ of opposite sign. The complicated magnetic structure is reasonably explained in accord to the space-group 136. The structural phase transition which transforms space-group 127 to space-group 136 is allowed to be continuous either by Landau theory or by renormalization-group theory, and available experimental data appear to be consistent with this assignment.

The description of the distorted structure below T_Q, which is given here in terms of space-group 136 together with an ordering of $4f$ quadrupole moments, is disputed by Matsumura *et al.*[13], on the grounds that the space-group appears to allow strong nonresonant (Thomson) reflections that are not observed. However, the intensity estimates quoted by Matsumura *et al.* for reflections ($h\,h\,l$) with l a half-integer arise from questionable assumptions. First, a 10% displacement at the phase transition in B and C positions and secondly, a uniform sign of the displacements whereas more realistic displacements are likely to be less than 1% in magnitude (on passing through T_Q crystals of DyB_2C_2 do not shatter which is what might be anticipated from a 10% displacement) and B and C displacements of opposite sign have to be considered. Taking both these factors into account dramatically reduces calculated intensities and, most importantly, revised values are in accord with recent observations by Adachi *et al.*[3] Furthermore, the distorted structure proposed by Matsumura *et al.*, which invokes a periodic displacement of Dy ions, is found to be consistent with Dy ions at sites ($4e$) in space-group 128 ($P4/mnc$). In this space-group the reflections ($h\,h\,l$) with l half-integer observed by Adachi *et al.* are forbidden, whereas they are allowed in space-group 136. (The lattice constant along c axis in both space-groups is twice of that in space-group 127.) Additionally, the space-group 128 ($P4/mnc$) will not support nonzero off-diagonal quadruple moments, e.g., $\langle Q_{xy} \rangle$ and $\langle Q_{xx} - Q_{yy} \rangle$, because Dy sites ($4e$) in space-group 128 have C_4 symmetry. In consequence, a periodic displacement of Dy ions does not fulfill the necessary condition for ordered Dy quadrupoles.

In the present analysis of resonant x-ray Bragg diffraction the mutipoles are mean values of atomic spherical tensor operators. The operators are specified and mean values, equivalent to a time average, may be obtained from particu-

lar models. For example, the time-odd atomic tensor of lowest order is of rank one. It is proportional to the magnetic moment, which might be derived from a Heisenberg model of the Dy spin moments. In more intricate systems the appropriate models can involve interactions of multipoles of rank higher than one. Such is thought to be the case for CeB$_6$.[14] Saturation values of multipoles can be derived from the ground-state wave function, just as one derives the saturation magnetic moment $\mu_0 = g\langle J\rangle$ by calculating the mean value of the angular momentum operator J.

Most previous interpretations of resonant x-ray Bragg diffraction have borrowed standard Cartesian tensor algebra from crystal physics.[15] The tensors are restricted by point-group symmetry. For example, electric quadrupole ($E2$) scattering events are represented by 81 variables; monoclinic symmetry restricts these to no more than 13 independent variables, and cubic symmetry restricts them to no more than 3 variables. A linear combination of spherical tensors, that are used in the present work, represents a Cartesian tensor in which point-group symmetry places restrictions on the coefficients in the expansion.

II. SCATTERING LENGTH

The x-ray scattering length f developed in a power series in $\tau = E/m_e c^2$ at the first level of approximation, contains diffraction from spin magnetic moments that add to Thomson scattering. We denote by $\mathbf{F}_s(\mathbf{k})$ and $F_c(\mathbf{k})$ the structure factors for spin and Thomson scattering, where the scattering wave vector $\mathbf{k} = \mathbf{q} - \mathbf{q}'$. The polarization dependences of spin and Thomson scattering are given by $\boldsymbol{\varepsilon}' \times \boldsymbol{\varepsilon}$ and $\boldsymbol{\varepsilon}' \cdot \boldsymbol{\varepsilon}$, respectively, where $\boldsymbol{\varepsilon}'$ and $\boldsymbol{\varepsilon}$ are the secondary and primary polarization vectors (here they are taken to be purely real, and the average value of $\boldsymbol{\varepsilon}' \times \boldsymbol{\varepsilon}$ in the limit of forward scattering is proportional to the helicity of the x-ray beam). Additionally, at the first level of approximation in τ the scattering length contains energy dependent terms that can enhance the diffraction signal by a resonance event. Scattering is caused by matrix elements of the current operator,

$$\mathbf{J}(\mathbf{q}) = \sum_j \ (\mathbf{p}_j + i\hbar \mathbf{s}_j \times \mathbf{q}) \exp(i\mathbf{q}\cdot\mathbf{R}_j), \qquad (2.1)$$

where $\mathbf{p}_j$, $\mathbf{R}_j$, and $\mathbf{s}_j$, respectively, are the operators for the momentum, position and spin of the electron labeled j.

An appropriate expression for the scattering length, in units of the classical radius of the electron, is

$$f = -\left\{ \boldsymbol{\varepsilon}'\cdot\boldsymbol{\varepsilon}F_c(\mathbf{k}) - i\tau(\boldsymbol{\varepsilon}'\times\boldsymbol{\varepsilon})\cdot\mathbf{F}_s(\mathbf{k}) \right.$$
$$+ \frac{1}{m_e}\sum_{\alpha\beta}\sum_\eta \ \varepsilon'_\alpha\varepsilon_\beta \left[\frac{W_\eta^{\alpha\beta}(\mathbf{q},\mathbf{q}')}{E - \Delta_\eta + \frac{i}{2}\Gamma_\eta} \right.$$
$$\left.\left.- \frac{W_\eta^{\alpha\beta}(-\mathbf{q},-\mathbf{q}')^*}{E + \Delta_\eta} \right]\right\}. \qquad (2.2)$$

In this expression, intermediate states of the resonant ion are labeled by η and the current matrix element is denoted by

$$W_\eta^{\alpha\beta}(\mathbf{q},\mathbf{q}') = \langle\{J_\alpha(-\mathbf{q}')|\eta\rangle\langle\eta|J_\beta(\mathbf{q})\}\rangle, \qquad (2.3)$$

where angular brackets denote the mean value of the enclosed quantity. In the limit of a high x-ray energy, well clear of resonance energies Δ_η, current operators contribute to f scattering by orbital and spin magnetic moments, and the spin adds to the contribution shown explicitly in Eq. (2.2). Another extreme limit of f as a function of primary x-ray energy E is obtained by matching E to a resonance energy. With suitable values of Γ_η and $W_\eta^{\alpha\beta}$, the limit $E = \Delta_\eta$ produces a term which dominates all other contributions to f. The matrix elements $W_\eta^{\alpha\beta}(\mathbf{q},\mathbf{q}')$ are usually developed in powers of $\mathbf{q}$ and $\mathbf{q}'$ and successive terms describe electric dipole ($E1$), electric quadrupole ($E2$), and magnetic dipole events. All the evidence from resonantly enhanced diffraction has been interpreted in terms of electric events, for magnetic events are typically a factor 1/137 smaller. At intermediate energies, excluding the two extreme cases already discussed, scattering will usually be determined by the full expression for f given in Eq. (2.2), which is itself correct at the first level in $\tau = E/m_e c^2$. Recent discussions[16] of diffraction by NiO in the vicinity of the Ni K edge[17] use an incorrect expressions for the scattering length, in which the purely magnetic contribution is different from the one shown in Eq. (2.2) and proportional to $\mathbf{F}_s(\mathbf{k})$.

III. STRUCTURE FACTORS

Structure factors for Dy ions contributing to Thomson diffraction and resonantly enhanced diffraction at space-group forbidden reflections are conveniently constructed with atomic spherical tensors $\langle T_q^{(K)}\rangle$. Here, K is a positive integer that labels the tensor rank, $-K \leq q \leq K$, and angular brackets denote a mean value of the enclosed operator. In the case of DyB$_2$C$_2$, the chemical and magnetic structures restrict $K + q$ to even integers, and odd-rank tensors always vanish in the absence of an applied magnetic field or magnetic long-range order. The maximum K for Thomson diffraction is $K = 6$, while $E1$ ($E2$) resonance events are described by tensors of ranks $K = 0$, 1 and 2 (0,1, . . . ,4).

A basic quantity $\Psi_q^{(K)}$ is the linear combination of the four Dy ion tensors with relative signs fixed by the Bragg condition ($h \ k \ l$). Following the development provided by Lovesey and Knight[18] one finds the following:

(a) $h + k$ odd and $l = n/2$,

$$\Psi_q^{(K)} = f_1 - f_2 - f_3 + f_4 = (1 - v_q)(\langle T_q^{(K)}\rangle - v_q\langle T_{-q}^{(K)}\rangle), \qquad (3.1)$$

with $v_q = \exp(i\pi q/2)$.

(b) $h + k$ even and $l = n/2$,

$$\Psi_q^{(K)} = f_1 + f_2 - f_3 - f_4 = (1 - v_q)(\langle T_q^{(K)}\rangle + v_q\langle T_{-q}^{(K)}\rangle). \qquad (3.2)$$

A necessary condition for diffraction is $v_q \neq +1$. Here, Dy atoms labeled by 1, 2, 3, and 4 are shown in Fig. 1.
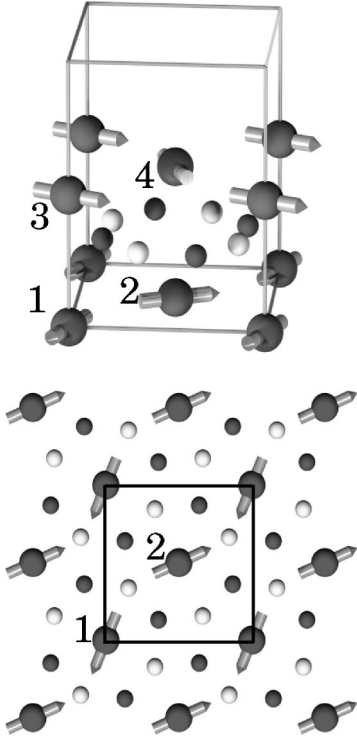
FIG. 1. The upper panel illustrates the sites of Dy ($4c$), B ($8j$), and C ($8j$) atoms in the unit cell of space-group $P4_2/mnm$ (136). Black spheres, white ones, ones with arrows represent B, C, and Dy atoms, respectively. The lower shows the network of B and C atoms at $z \simeq 1/4$ and the Dy plane at $z = 0$. Arrows show the magnetic configuration of Dy ions below T_C.

For Thomson diffraction and resonant diffraction by paramagnetic ions ($T > T_C$) K is an even integer, and allowed $q = 0, \pm 2, \pm 4, \pm 6$. However, a necessary condition $\nu_q = -1$ restricts q to $\pm 2, \pm 6$. The component $q = 0$ is absent because we consider space-group forbidden reflections.

Thomson diffraction at these Bragg reflections arises from spatial anisotropy in the $4f$ valence shell.[14] We find,

(a$'$)

$$F_c \propto (\hat{k}_a^2 - \hat{k}_b^2)\{\langle j_2 \rangle \langle Q_{aa} - Q_{bb} \rangle + \cdots \}, \qquad (3.3)$$

where $\hat{\mathbf{k}} = \mathbf{k}/k \propto (h\,k\,l)$, $\langle Q_{\alpha\beta} \rangle$ are components of the Dy $4f$ quadrupole derived as indicated Eq. (3.11) from $\langle T_q^{(2)} \rangle_c$, and $\langle j_m \rangle$ are spherical Bessel function transforms of the $4f$ radial distribution. Dots in Eq. (3.3) stand for terms that contain $\mathrm{Re}\langle T_2^{(4)} \rangle_c$, $\mathrm{Re}\langle T_2^{(6)} \rangle_c$, and $\mathrm{Re}\langle T_6^{(6)} \rangle_c$.

(b$'$) The second case of interest is

$$F_c \propto \hat{k}_a \hat{k}_b \{\langle j_2 \rangle \langle Q_{ab} \rangle + \cdots \}, \qquad (3.4)$$

and the admitted term contain the imaginary parts of $\langle T_2^{(4)} \rangle_c$, $\langle T_2^{(6)} \rangle_c$, and $\langle T_6^{(6)} \rangle_c$.

Contributions from B and C ions to the Thomson diffraction in question are related to their fractional displacements δ along the c axis which accompany the structural phase transition at T_Q. The h, k, l dependence of each contribution is

$$\sin(\pi l)\sin(2\pi l \delta)\sin\left[\frac{\pi}{2}\{h + k(1 - 4x)\}\right]$$

$$\times \sin\left[\frac{\pi}{2}\{k - h(1 - 4x)\}\right]. \qquad (3.5)$$

The available experimental data[3] suggests $|\delta| \sim 1/1000$ and δs for B and C are of opposite sign.

The resonant enhancement can be interpreted in terms of the coherent sum of two oscillators for $E1$ and $E2$ transitions, which is shown in Sec. V. Following Eq. (2.2), each oscillator is defined by a resonance energy Δ and a width Γ, and the corresponding scattering length is,

$$f_{\mu\nu} = \frac{F_{\mu\nu}^{(E1)}(hkl)}{E - \Delta_1 + \frac{i}{2}\Gamma_1} + r\frac{F_{\mu\nu}^{(E2)}(hkl)}{E - \Delta_2 + \frac{i}{2}\Gamma_2}. \qquad (3.6)$$

In this expression μ and ν label the secondary and primary polarizations, respectively, r is the mixing parameter, and $F_{\mu\nu}^{(E1)}(hkl)$ and $F_{\mu\nu}^{(E2)}(hkl)$ are the structure factors for $E1$ and $E2$ enhanced diffraction, expressed in terms of mean values of atomic tensors denoted by $\langle T_q^{(K)} \rangle$.

Scattering enhanced by an $E1$ event at $(0\,0\,l)$ reflections contains only $\langle T_q^{(2)} \rangle$. One finds the following:

$$F_{\sigma'\sigma}^{(E1)}(0\,0\,l) = 4\sin(2\Psi)\mathrm{Im}\langle T_{+2}^{(2)} \rangle_d, \qquad (3.7)$$

$$F_{\pi'\sigma}^{(E1)}(0\,0\,l) = -4\sin\theta\cos(2\Psi)\mathrm{Im}\langle T_{+2}^{(2)} \rangle_d. \qquad (3.8)$$

In these expressions we have added a subscript d to atomic tensors to indicate that absorption at the $2p$ edge and an $E1$ event leads to a sensitivity to d-like, presumably strongly $5d$, valence states. The dependences of $E1$ structure factors on the azimuthal angle Ψ and the Bragg angle θ are consistent with results reported by Tanaka *et al.*[4]

Results[18] of the structure factors for an $E2$ event are

$$F_{\sigma'\sigma}^{(E2)}(0\,0\,l) = \sin^2\theta\sin(2\Psi)\mathrm{Im}\langle 3\sqrt{2}T_{+2}^{(2)} - \sqrt{11}T_{+2}^{(4)} \rangle, \qquad (3.9)$$

$$F_{\pi'\sigma}^{(E2)}(0\,0\,l) = -\sin\theta\cos(2\Psi)\mathrm{Im}\langle 3\sqrt{2}T_{+2}^{(2)}(3 - 4\sin^2\theta)$$

$$+ \tfrac{1}{2}\sqrt{11}T_{+2}^{(4)}(1 + \sin^2\theta) \rangle. \qquad (3.10)$$

The structure factors are linear combinations of the imaginary parts of $\langle T_{+2}^{(2)} \rangle$ and $\langle T_{+2}^{(4)} \rangle$, and these atomic tensors describe properties of the Dy $4f$ valence shell. We note that

$$\langle T_{+2}^{(2)} \rangle = \frac{1}{\sqrt{6}}\langle T_{xx}^{(2)} - T_{yy}^{(2)} + 2iT_{xy}^{(2)} \rangle \propto \langle Q_{aa} - Q_{bb} + 2iQ_{ab} \rangle, \qquad (3.11)$$

where the Cartesian tensors $\langle T_{\alpha\beta}^{(2)} \rangle$ are purely real. $F_{\mu\nu}^{(2)}(0\,0\,l)$ contains a component of the quadrupole moment $\langle T_{xy}^{(2)} \rangle \propto \langle Q_{xy} \rangle$ and that of the hexadecapole $\mathrm{Im}\langle T_{+2}^{(4)} \rangle$, and all contributions transform according to the representation A_g of $2/m$.

IV. EXPERIMENTAL METHOD

Two series of resonant x-ray diffraction (RXD) experiments, from which preliminary data have been reported,[4] were carried out at the bending magnet beam line 4C in the Photon Factory (PF), KEK, Japan. One further RXD experiment with a polarization analyzer at the ID20 magnetic scattering undulator beam line[19] in the European Synchrotron Radiation Facility (ESRF), France, was performed. The components of optics in both facilities were almost the same. A Si (111) double-crystal monochromator followed by a focusing bent cylindrical mirror to cut higher harmonic x-rays was used in PF, while a Si (111) double-crystal monochromator located between two focusing mirrors was used in ESRF. The incident x-rays of a high degree of linear σ polarization having its energy in the vicinity of the Dy L_{III} absorption edge were used. The energy resolution in the experiments at PF and that at ESRF was ~ 2.3 eV and ~ 1.6 eV, respectively. In addition, a highly oriented pyrolytic graphite (HOPG) crystal analyzer to separate the σ', and π' components of the x-ray beam diffracted by the sample was used in the experiment in ESRF. The scattering angle 90.77° (2θ) at HOPG (006) reflection for the Dy L_{III} absorption edge, where the ratio of the intensity in the π'-σ channel to that in the σ'-σ channel at DyB_2C_2 Bragg (002) reflection is 1×10^{-3}, gives almost perfect polarization analysis.[20]

The samples were prepared with highly pure Dy (99.9%), B (99.8%), and C (99.999%). First, compounds were synthesized by the conventional argon arc technique, and then, single crystals of DyB_2C_2 were grown by the Czochralski method using a tri-arc furnace. The crystals were checked with powder x-ray diffraction, of which patterns showed that the compounds had a single phase. The mosaic spread of the single crystal used for this work in ESRF was about 0.07° in FWHM within an area of 1×0.8 mm^2. The slit aperture was limited to 0.05×0.05 mm^2 in size. The sample in size of about $3 \times 3.5 \times 0.6$ mm^3 was mounted with bees-wax in a closed cycle ^{4}He refrigerator, and was aligned so that the c axis, which is perpendicular to a cleavage plane, was almost parallel to the ϕ axis of the six-axis diffractometer to perform azimuthal angle scans around the scattering vector.

V. EXPERIMENTAL RESULTS

We have observed forbidden reflections of $(0\,0\,l)$ with $l = n/2$ and $n = 1,3,5$, and $(1, 0, 1/2)$. In the following sections, we show the energy dependence, azimuthal angle dependence, and temperature dependence of the intensities of the forbidden reflections.

A. Energy dependence

Figure 2 shows the energy dependence of the intensities of the $(0\,0\,3/2)$, $(0\,0\,5/2)$, and $(1\,0\,1/2)$ reflections together with the $(0\,0\,2)$ Bragg reflection. The azimuthal-angle Ψ is defined by the angle between the a axis and the scattering plane (the plane which includes the wave vector $\mathbf{q}$ of the incident beam and the wave vector $\mathbf{q}'$ of the diffracted beam).
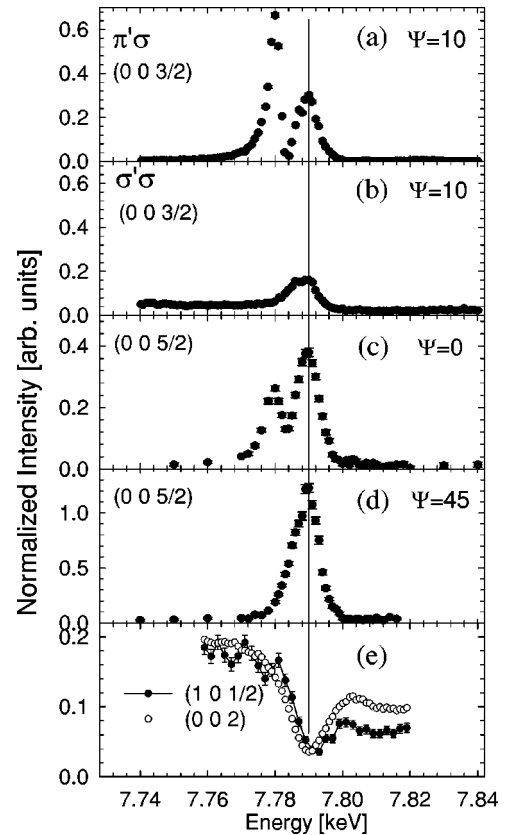

FIG. 2. Energy dependence of (a) the intensity of the $(0\,0\,3/2)$ reflection at $\Psi = 10$ for the $\pi' - \sigma$ channel, (b) that for the $\sigma' - \sigma$ channel, (c) the integrated intensity in ω scans of the $(0\,0\,5/2)$ at $\Psi = 0$, and (d) that at $\Psi = 45$, and (e) intensity of the $(1\,0\,1/2)$ together with that of the $(0\,0\,2)$ Bragg reflection. All intensities are normalized by the monitor counts. Here, (a) and (b) were measured at the ESRF with an energy resolution ~ 1.6 eV at 17 K with polarization analysis, and (c), (d), and (e) were measured in PF with a resolution ~ 2.3 eV at 17 K without any polarization analysis.

The results are summarized as follows. (i) The intensity of the $(1\,0\,1/2)$ reflection has a similar energy dependence as that of the $(0\,0\,2)$ Bragg reflection as shown in (e). (ii) There are two clear resonant signals observed at 7.790 keV and 7.780 keV as shown in panel (a) and (c): (a) the intensity of the reflection $(0\,0\,3/2)$ reflection for the $\pi' - \sigma$ channel measured at azimuthal angle $\Psi = 10$, (c) the integrated intensity of the $(0\,0\,5/2)$ reflection measured at $\Psi = 0$ with no polarization analysis. The position of the maximum intensity at 7.790 keV corresponds to that of the minimum of the intensity of $(0\,0\,2)$ Bragg and $(1\,0\,1/2)$ forbidden reflections. (iii) At $\Psi = 45$, only one resonant enhancement is observed as shown in (d). (iv) A shift of the polarization in the resonant diffraction is observed in the intensity of $(0\,0\,3/2)$ reflection at $\Psi = 10$ as shown in (a) and (b). (v) Two peaks in Fig. 2(a) at 7.790 keV and at 7.780 keV can be fit by Lorentz functions having an 4.2-eV half width at half maximum (HWHM), and a 2.3-eV HWHM, respectively.

B. Azimuthal angle dependence

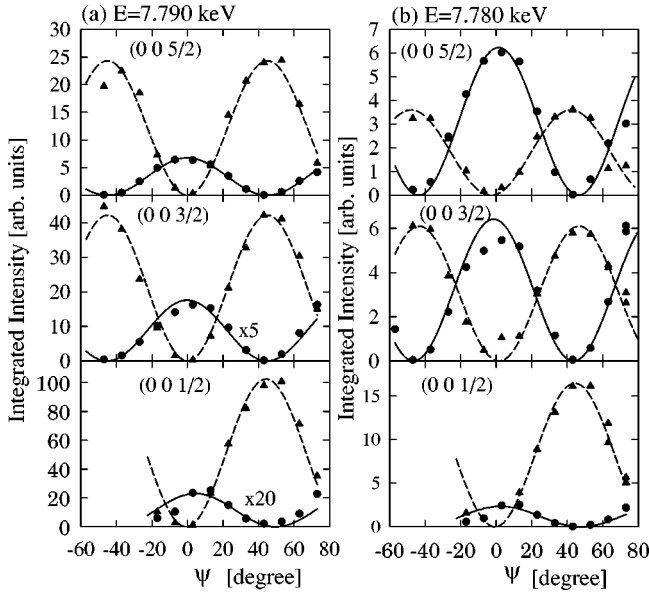The azimuthal angle dependence has been measured with polarization analysis at the ESRF. As described in Sec. I, it is

FIG. 3. Change of the integrated intensities with the rotation of sample around the reflection vectors, (0 0 1/2), (0 0 3/2), and (0 0 5/2) at (a) 7.790 keV and at (b) 7.780 keV. Azimuthal angle Ψ is defined by the angle between the a axis and the scattering plane. Circles (triangles) represent the signal through the $\pi' - \sigma$ ($\sigma' - \sigma$) channel. The full curves and broken curves are squared sinusoidal functions which are fit to each of the data.

important to do the experiment at the energy of $E2$ transition in terms of *direct* observation of AFQ moment ordering, and we therefore measured azimuthal angle dependence at two energy positions, 7.790 keV and 7.780 keV. Figure 3 shows the azimuthal angle dependence of the integrated intensities in ω scans measured at three reflections, (0 0 1/2), (0 0 3/2), and (0 0 5/2).

The results are summarized as follows. (i) Each azimuthal angle scan has $\pi/2$ period. (ii) The intensities in two polarization channels $\pi' - \sigma$ and $\sigma' - \sigma$ are antiphase. (iii) The ratio of the intensity for the $\pi' - \sigma$ channel to that for the $\sigma' - \sigma$ channel differs for the indices of the reflections and for resonant energies.

Finally, we point out that the intensities shown in Fig. 2 are consistent with the results of the azimuthal angle scans. Panel (c) in Fig. 2 is compared with the top two panels in Fig. 3, where the intensity in the $\pi' - \sigma$ channel (circles) is dominant at $\Psi = 0$ at two energies (7.790 and 7.780 keV). Similarly, panel (d) in Fig. 2 is compared with the top two panels in Fig. 3, where the intensity in the $\sigma' - \sigma$ channel (triangles) is dominant at $\Psi = 45$ at both energies. It is concluded that panels (c) and (d) in Fig. 2 show the intensity in the $\pi' - \sigma$ and the $\sigma' - \sigma$ channels, respectively. [Note that (c) and (d) were measured without any polarization analysis.] Panels (a) and (b) in Fig. 2 are also consistent with the middle two panels in Fig. 3. The intensity in the $\pi' - \sigma$ channel is dominant at both energies when $\Psi = 10$.

Here, it is important to note that no obvious enhanced signals in the $\sigma' - \sigma$ channel is observed at 7.780 keV as shown in Fig. 2. [See panel (b) and (d). The intensity shown in panel (c) is attributed to the $\pi' - \sigma$ channel as explained
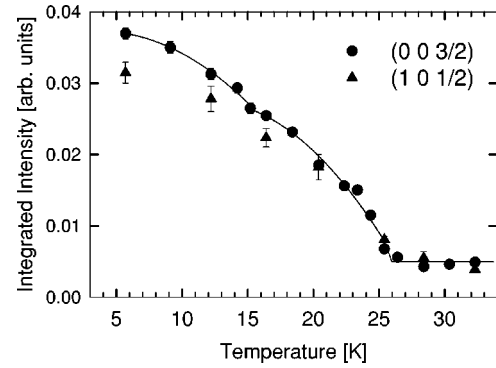
above.] Therefore the intensity for the $\sigma' - \sigma$ channel measured at 7.780 keV shown in panel (b) in Fig. 3 seems to be attributed to the tail of the enhancement at 7.790 keV.

We discuss this matter together with the ratios of the intensity in the two channels in Sec. VI, where we give a clear evidence that the resonant enhancement at 7.780 keV is due to the $E2$ transition from $2p$ to $4f$ valence shell.

C. Temperature dependence

Figure 4 shows the temperature dependence of the integrated intensity of the reflections at (0 0 3/2) and (1 0 1/2) measured with the incident x rays of $E = 7.790$ keV in PF. The intensities of two reflections increase as temperature decreases below $T_Q = 25$ K, obviously indicating that two reflections are caused by the transition at T_Q, which has been observed in the specific heat measurement.[12] The small intensity above 25 K is attributed to higher harmonic components of the incident x rays. It seems that the intensity of the reflection (0 0 3/2) has a step around 15 K ($\sim T_C$). Further increase in the intensity below T_C can be attributed to magnetic resonant scattering. A detailed discussion on the onset of quadrupole ordering in DyB$_2$C$_2$ has been given elsewhere.[21]

VI. DISCUSSION

Although the crystal symmetry below T_Q and configuration of the AFQ moments has been described in the previous paper,[4] we give more detail discussions in the following three sections. Finally we give discussions of quadrupole and hexadecapole moment ordering.

A. Space group

Let us start by considering data collected at $h + k$ odd and $l = n/2$ with n equal to an odd integer. Data in Fig. 2(e) demonstrate that the forbidden (1 0 1/2) and allowed (0 0 2) reflections have essentially the same dependence on energy and minimum intensity occurs at $E = 7.790$ keV. (Here we refer to extinction rules for the room temperature crystal structure $P4/mbm$.) Diffraction signals are strongly influenced by absorption at the L_{III} edge. Consequently, this re-

flection includes Thomson scattering observed in usual diffraction experiments performed at energies far above atomic resonances. Further, the intensity of the (1 0 1/2) reflection increases as temperature decreases below T_Q as well as that of the (0 0 3/2) reflection as shown in Fig. 4. This finding implies that a structural phase transition accompanies an ordering of Dy multipoles. (As we discuss later the reflections (0 0 l) with l a half-integer arise from quadrupole and hexadecapole moment ordering.)

These facts, however, are not enough to conclude that a structural phase transition accompanies the transition at T_Q, because the spatial anisotropy in the Dy $4f$ valence shell in the ordered state can also contribute to the intensity of the (1 0 1/2) reflection as described in Eq. (3.3) in Sec. III. We show two more strong reasons why we conclude that a structural phase transition arises at T_Q. If the space-group 127 ($P4/mbm$) remains in the AFQ ordering state, the point-group symmetry of Dy sites is $4/m$ which allows $q = 0, \pm 4$, and according to Eq. (3.2) both these values give null intensity at (0 0 l) with l half-integer. This result conflicts with our observations. The second reason is about the intensities of reflections of (h 0 l) and (h h l) with l half-integer measured in the nonresonant regime observed by Adachi et al.[3] As they discussed, the intensities are one or two orders of magnitude larger than the value expected for Dy quadrupole moment. Consequently, we conclude that a lattice distortion accompanies with the transition at T_Q. Which space-group matches all the results on the ordered state in DyB_2C_2? The necessary conditions are (i) the lattice constant along the c axis is twice of that above T_Q ($c' = 2c$), (ii) the local symmetry of Dy ions is not four but two-fold symmetry. Only space-group 136 ($P4_2/mnm$) satisfies the above conditions. As described in Sec. I, space-group 128 ($P4/mnc$), which Matsumura et al.[13] have suggested, does not fulfill condition (ii), and additionally, the extinction rule for reflections (h h l) with l half-integer.

The local symmetry of Dy ions in space-group 136, where the point-group symmetry of Dy sites ($4c$) is $2/m$, which allows $q = 0, \pm 2$, is capable of producing both (0 0 l) and (h 0 l) reflections with h odd and l half-integer according to Eqs. (3.1) and (3.2). Moreover, inspection of the Thomson structure factors recorded in the Sec. III shows that there are contributions at (1 0 l) from anisotropy in the Dy $4f$ shell, and the B and C ions displaced from the room temperature structure. Note that the Dy, B, and C contributions to the (1 0 1/2) reflection all originate from the lattice distortion that sets in at T_Q; the Dy contribution comes from the reduction in site symmetry to $2/m$ from $4/m$, and contributions from B and C come from their displacements along the c axis.

B. Multipole ordering motif

Figure 5 shows a structural model of the AFQ ordering in space-group 136 below T_Q. It is important to note that we can deduce the configuration of Dy multipole moments, which reflect the local atomic structure, by taking account of space-group symmetry operations and that we do not need to refer the magnetic structure below T_C.
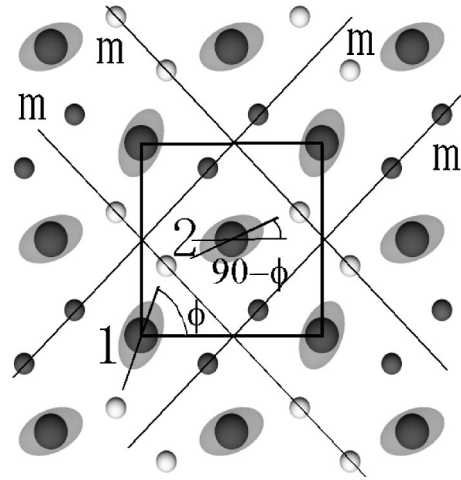

FIG. 5. A diagram of AFQ ordering in space-group 136. The plane of Dy ions ($4c$) with the anisotropic electron clouds at $z = 0$ and the plane of B ($8j$) and C ($8j$) network (only B atoms are shown for convenience) at $z \simeq 1/4$ are illustrated. Dark (light) B atoms are slightly below (above) the $z = 1/4$ plane. Here z is represented on a scale of the lattice constant of the c axis of space-group 136. A unit cell is shown by thick lines. Mirror planes marked by letters "m" are shown by thin lines.

Ion 1 and its neighboring ions along the c axis are related by a rotation of $\pi/2$. A similar identity holds for ions 2 and its neighboring ions along the c axis. The ions 1 and 2 are related by reflection in a mirror plane. This configuration provides the relations of the atomic tensors for ions 1, 2, 3, and 4 (labels are given in Fig. 1): $\langle T_q^{(K)}(3)\rangle = \exp(iq\pi/2)\langle T_q^{(K)}(1)\rangle$ and $\langle T_q^{(K)}(2)\rangle = \exp(iq\pi/2)\langle T_{-q}^{(K)}(1)\rangle$. The structure factors for the forbidden reflections in Eqs. (3.1) and (3.2) are given with these relations. This configuration of Dy multipoles, of course, matches the magnetic structure shown in Fig. 1.

We summarize the correlation between the multipole moments and the lattice distortions. The correlation should accord with Neumann's principle, which is introduced in Sec. I. Considering the (1 0 1/2) reflection leads us to conclude that the space group below T_Q is 136 ($P4_2/mnm$), where the point-group symmetry of Dy ions is $2/m$, which allows $q = 0, \pm 2$. This local symmetry supports nonzero off-diagonal quadrupole $\langle Q_{xy}\rangle$ and $\langle Q_{xx} - Q_{yy}\rangle$ where the Cartesian axes x and y lie in the plane normal to the crystal c axis and the axis of two-fold rotation symmetry in $2/m$. Furthermore, the correlation is kept during the transition as shown in the temperature dependence (Fig. 4) of the integrated intensity of the reflections at (0 0 3/2) and (1 0 1/2), which indicates that the structural phase transition which transforms space-group 127 to space-group 136 is continuous, and that the AFQ ordering transition appears simultaneously.

C. Ordering of quadrupole and hexadecapole moments

Turning next to reflections with $h + k$ even, our Thomson structure factors for Dy, B, and C are zero at $h = k = 0$. In consequence, the resonantly enhanced signals at $h = k = 0$

TABLE I. The ratio $(I_{\pi'\sigma}/I_{\sigma'\sigma})$ of intensity in the $\pi'-\sigma$ and the $\sigma'-\sigma$ channels obtained by fitting with $\sin^2 2\Psi$. The last column records the value of the mixing parameter.

Reflection	$\sin^2\theta$	7.790 keV ($E1$)	7.780 keV ($E2$)	r'
0 0 5/2	0.315	0.278	1.73	1.060
0 0 3/2	0.113	0.083	1.04	1.059
0 0 1/2	0.013	0.011	0.14	1.053

and at (1 0 1/2), displayed in Fig. 2, are profoundly different. There are two clear resonant signals, as shown in panel (a) and (c) of Fig. 2. The resonant enhancement at 7.790 keV is attributed to the electric dipole transition $2p_{3/2}$ to $5d$ ($E1$) because the maximum locates at the same position of the minimum of (0 0 2) Bragg reflection due to the L_{III} absorption. The enhancement at 7.780 keV, which has narrower width, is attributed to the electric quadrupole transition $2p_{3/2}$ to $4f$ ($E2$) for the following reasons.

We discuss the intensities observed as a function of the azimuthal angle Ψ with a help of the theoretical prediction shown by Eqs. (3.7)–(3.10). The data for azimuthal angle scans at (0 0 l) with $l = 1/2$, 3/2, and 5/2 are shown in Fig. 3, separately for the $\pi'-\sigma$ (rotated) and the $\sigma'-\sigma$ (unrotated) channels of scattering. The right (left) panel in Fig. 3 is derived from intensity at $E = 7.780$ keV (7.790 keV). Ratios of the intensity in the $\pi'-\sigma$ and the $\sigma'-\sigma$ channels $(I_{\pi'\sigma}/I_{\sigma'\sigma})$ for both resonant energies are summarized in Table I. Here θ is the Bragg angle for each reflection, and r' is the mixing parameter which is defined in Eq. (6.4). The absorption effect is neglected because it does not matter when comparing values of the parameter among like reflections.

Eqs. (3.7) and (3.8) for $F^{(E1)}_{\pi'\sigma}(0\,0\,l)$ and $F^{(E1)}_{\sigma'\sigma}(0\,0\,l)$ predict that the ratio of the intensity in the $E1$ rotated channel to that in the unrotated one is proportional to $\sin^2\theta$. Our data (the ratios at 7.790 keV) for three reflections are in total agreement with this prediction. Hence, this fact leads us to conclude that the resonant enhancement at 7.790 keV is due to the $E1$ transition and that the azimuthal dependence shows the ordering of the quadrupole moment ($\mathrm{Im}\langle T^{(2)}_{+2}\rangle_d \neq 0$) of the $5d$ valence state.

However, we cannot directly discuss the multipole moment ordering of Dy $4f$ valence shell at this resonant energy ($E1$) because the $5d$ state of Dy ions can be hybridized with the outer electrons of the surrounding B and C atoms. Recently, Igarashi *et al.*[22] calculated the intensity observed at the $E1$ transition by treating the $5d$ state as a band and the $4f$ valence state as localized, and showed that the contribution of the charge anisotropy of the $4f$ state to the quadrupole moment of the $5d$ state through the $5d$-$4f$ Coulomb interaction is much smaller than that of the lattice distortion of B and C atoms through the hybridization with the $2p$, $3s$ states of B and C atoms.

As described in Sec. I, the intermediate states probed by the resonance need to be the same as the states which directly drive the ordering. In other words, we can show a direct evidence of multipole moment ordering of the Dy $4f$

valence shell only by the resonant enhancement by an $E2$ event and the azimuthal angle dependence of the reflections at this energy.

Let us discuss the possibility of the $E2$ resonance ($2p \rightarrow 4f$) scattering at 7.780 keV. The ratios for 7.780 keV have completely different dependence on the reflection indices, which indicates that the enhancement at 7.780 keV cannot be attributed to the $E1$ transition. Note that the scattering length of the general resonant scattering theory up to electric quadrupole transition includes dipole-dipole, dipole-quadrupole hybridization and quadrupole-quadrupole terms. The first term corresponds to the $E1$ transition as described above. The second term vanishes in the presence of inversion symmetry which applies to Dy ions in the space-group to 136. Hence, only pure quadrupole ($E2$) events are taken into account for the enhancement at 7.780 keV.

We need to employ Eq. (3.6) and a mixing parameter for a precise discussion because the two resonantly enhanced signals are not separated in energy as shown in Fig. 2. The tail of the lower-energy side of the enhanced signals at 7.790 keV overlaps the peak of the enhancement of 7.780 keV lightly because of the broad energy width. This fact suggests that, the integrated intensity of the azimuthal angle scan in the $\sigma'-\sigma$ channel at 7.780 keV may be attributed to the tail of the enhanced signals at 7.790 keV described in Sec. V.

The structure factor at 7.780 keV is found by putting $E = \Delta_2$,

$$|f_{\mu\nu}|^2 = \left| \frac{F^{(E1)}_{\mu\nu}}{\Delta_2 - \Delta_1 + \dfrac{i}{2}\Gamma_1} - r\frac{2i}{\Gamma_2}F^{(E2)}_{\mu\nu} \right|^2, \qquad (6.1)$$

where $\Delta_2 = 7.780$ keV and $\Delta_1 = 7.790$ keV.

Using Eqs. (3.7)–(3.10) gives the structure factor for each channel,

$$\frac{|f_{\sigma'\sigma}|^2}{A} = 1 + r'^2\sin^4\theta(1-p)^2 - 2r'B\sin^2\theta(1-p). \tag{6.2}$$

$$\frac{|f_{\pi'\sigma}|^2}{A} = \sin^2\theta[1 + r'^2C^2 - 2r'BC], \qquad (6.3)$$

where

$$A = 16\{\mathrm{Im}\langle T^{(2)}_{+2}\rangle_d\}^2\left\{\Delta^2 + \left(\frac{\Gamma_1}{2}\right)^2\right\}^{-1},$$

$$B = \frac{\dfrac{1}{2}\Gamma_1}{\left\{\Delta^2 + \left(\dfrac{1}{2}\Gamma_1\right)^2\right\}^{1/2}},$$

$$C = (3 - 4\sin^2\theta) + \frac{p}{2}(1 + \sin^2\theta),$$

$$\Delta = \Delta_2 - \Delta_1.$$

Here we employ the prediction that the dependence of $E1$ and $E2$ events on the azimuthal angle Ψ is the same. There are two parameters, one is the mixing parameter r', and the other is $p \equiv \sqrt{11}\langle T_2^{(4)}\rangle'' / 3\sqrt{2}\langle T_2^{(2)}\rangle''$, and r' is defined as

$$r' \equiv -r \frac{\left\{\Delta^2 + \left(\frac{1}{2}\Gamma_1\right)^2\right\}^{1/2}}{\frac{1}{2}\Gamma_2} \cdot \frac{\mathrm{Im}3\sqrt{2}\langle T_{+2}^{(2)}\rangle}{4\,\mathrm{Im}\langle T_{+2}^{(2)}\rangle_d}. \qquad (6.4)$$

The ratio of Eqs. (6.2) and (6.3) and the experimental values of $I_{\pi'\sigma}/I_{\sigma'\sigma}$ in Table I give three equations with two parameters. In principle, a pair of the equations among three can be solved. By putting $\Delta = 10$ eV and $\Gamma_1/2 = 4.2$ eV, equations for (0 0 5/2) and (0 0 3/2) reflections give $r' = 1.05$ and $p = 1.025$, and those for (0 0 5/2) and (0 0 1/2) reflections give $r' = 1.03$ and $p = 1.12$, and those for (0 0 3/2) and (0 0 1/2) reflections give $r' = 0.94$ and $p = 1.77$. It is found that these equations give $r' \sim 1$ and $p \sim 1$ except of the last value of p.

One striking feature of our data in Fig. 2 is the absence in panels (b) and (d) of enhanced signals at $E = 7.780$ keV. As mentioned in Sec. V, taking account of data for azimuthal angle scans in Fig. 3 leads us to conclude that there is no obvious enhancement in the $\sigma' - \sigma$ channel at 7.780 keV. This is explained by a cancellation of the quadrupole and hexadecapole contributions to $F_{\sigma'\sigma}^{(E2)}(00l)$ achieved when $\mathrm{Im}\{3\sqrt{2}\langle T_2^{(2)}\rangle - \sqrt{11}\langle T_2^{(4)}\rangle\} \sim 0$ or $p \sim 1$. The result of the above calculations for the two parameters, particularly for p, is in excellent agreement with the experimental data observed in the energy dependence.

Conversely, the above analysis of the data of the azimuthal angle scans with the theoretical prediction for the $E2$ resonance predicts that the lack of resonant enhancement in the $\sigma' - \sigma$ channel at the $E2$ transition energy. This prediction for Dy $4f$ multipoles immediately accounts for the absence of an $E2$ signal in panel (b), and it also accounts for its absence in panel (d) on noting that the signal here is actually purely unrotated ($\sigma'\sigma$) since the rotated ($\pi'\sigma$) signal is negligible at $\Psi = 45$. Hereby, we take the parameter $p = 1$, and determine the parameter r', of which values are shown in Table I. The parameter r' is almost constant for each reflection indicating that data in the $E2$ rotated channel are in total agreement with the predicted behavior $\sin^2\theta\cos^4\theta$, which follows on taking account of the foregoing relation between the Dy $4f$ quadrupole and hexadecapole. [Putting $p = 1$ gives a term $\cos^2\theta$ in Eq. (3.10)].

Finally, we conclude that (i) the resonant enhancement at 7.780 keV is reasonably attributed to $E2$ transition, (ii) the azimuthal dependence shows the ordered state of the quadrupole and hexadecapole moments of the $4f$ valence shell, and (iii) the signals in the unrotated channel ($\sigma'\sigma$) cancel at the $E2$ transition energy due to a relation between Dy $4f$ quadrupole and hexadecapole moments ($\mathrm{Im}\{3\sqrt{2}\langle T_2^{(2)}\rangle - \sqrt{11}\langle T_2^{(4)}\rangle\} \sim 0$).

VII. DISCUSSION OF Dy $4f$ PROPERTIES

We will look at the conclusion, drawn from an analysis of data in the $E2$ channel, that contributions from the Dy $4f$ quadrupole and hexadecapole cancel out, which implies $\langle T_2^{(4)}\rangle'' \sim 3(2/11)^{1/2}\langle T_2^{(2)}\rangle''$. Taken together with other independent experimental results the conclusion enables us to make some headway in finding a description of the low energy states of the Dy ion.

Neutron spectroscopy performed on a sample with Dy diluted by Y shows that the Dy crystal potential has states at approximately 17 K and 48 K$\sim 2T_Q$ above the ground state.[23] This observation adds weight to the conjecture by Yamauchi *et al.*[12], based on data for the specific heat, that just two levels are essential in determining structural and magnetic properties, namely, the ground and first excited states. Such an energy level scheme immediately accounts for entropy $R\ln 2$ released at T_Q and T_C in data reported in Ref. 12.

Let the Dy ground state be spanned by the state $|\Psi\rangle$ and its Kramers conjugate $|\bar\Psi\rangle$, derived from $|\Psi\rangle$ by application of the time-reversal operator. The sixteen eigenstates of J_z are labeled $|M\rangle$, and the axis of quantization is parallel to the crystal c axis and the axis of $2/m$. We will show that in looking for a minimal model of Dy a suitable choice for $|\Psi\rangle$ is,

$$|\Psi\rangle = i\sin\theta\sin\varphi|M\rangle + \cos\theta|M-2\rangle + i\sin\theta\cos\varphi|M-4\rangle, \qquad (7.1)$$

where θ and ϕ are mixing angles. The linear combination of $|M\rangle$ respects the Dy site symmetry and the relative phases make $\langle\Psi|T_2^{(K)}|\Psi\rangle = \langle\bar\Psi|T_2^{(K)}|\bar\Psi\rangle$ purely imaginary. By the construction of $|\bar\Psi\rangle$ from $|\Psi\rangle$ one has $\langle\Psi|T_2^{(K)}|\bar\Psi\rangle = 0$. The states associated with the first excited level, about 17 K above the ground state, are $|\Psi_2\rangle$ and $|\bar\Psi_2\rangle$ and,

$$|\Psi_2\rangle = \cos\theta\sin\varphi|M\rangle + i\sin\theta|M-2\rangle + \cos\theta\cos\varphi|M-4\rangle. \qquad (7.2)$$

We have $\langle\Psi|\Psi_2\rangle = 0$ and $\langle\Psi|T_2^{(K)}|\Psi\rangle = -\langle\Psi_2|T_2^{(K)}|\Psi_2\rangle$. Requiring $\langle\Psi|T_2^{(K)}|\Psi_2\rangle = 0$ places one condition on the two mixing angles, and with $K = 2$, $|\Psi\rangle$ and $|\Psi_2\rangle$ span a space in which the quadrupole Q_{xy} behaves like an Ising spin (1/2) variable. The result $\langle T_2^{(4)}\rangle \sim 3(2/11)^{1/2}\langle T_2^{(2)}\rangle$ can be used as a second condition on the mixing angles, in which case the angles are completely determined.

Additional input to the model of Dy is gained from looking at the saturation magnet moment μ_0 developed in the ground state $|G\rangle$, which is a linear combination of $|\Psi\rangle$ and $|\bar\Psi\rangle$. Since $\langle\Psi|J_z|\bar\Psi\rangle = 0$ and $\langle\Psi|J_z|\Psi\rangle = -\langle\bar\Psi|J_z|\bar\Psi\rangle$ one has $\langle G|J_z|G\rangle = 0$. Thus, the moment is confined to the basal plane and subtends an angle $\tan^{-1}\{\langle G|J_y|G\rangle/\langle G|J_x|G\rangle\}$ with respect to the x axis, while

$$\mu_0 = \frac{4}{3}\{\langle G|J_x|G\rangle^2 + \langle G|J_y|G\rangle^2\}^{1/2}. \qquad (7.3)$$

With

$$|G\rangle = \frac{1}{\sqrt{2}}\{e^{i\delta}|\Psi\rangle + |\bar{\Psi}\rangle\}, \tag{7.4}$$

it follows that,

$$\langle G|J_\alpha|G\rangle = \mathrm{Re}\{e^{-i\delta}\langle\Psi|J_\alpha|\bar{\Psi}\rangle\}. \tag{7.5}$$

Requiring $\langle\Psi|J_\alpha|\bar{\Psi}\rangle$ to be different from zero limits choices for M. Experimental results for μ_0 lie between 7.1 and 8.8 (Yamauchi *et al.*[12]) and the canting angle $\sim 23°$, and these two bits of information are consistent with the choice $M = 5/2$.

By using values of the reduced matrix elements of $T_q^{(K)}$ for an $E2$ event at the Dy L_{III} absorption edge one finds, for $M = 5/2$, that the result $\langle T_2^{(4)}\rangle \sim 3(2/11)^{1/2}\langle T_2^{(2)}\rangle$ yields for the mixing angle φ the result $\tan\varphi \sim -0.9$.[24] Secondly, placing on $T_2^{(2)}$ the requirement $\langle\Psi|T_2^{(2)}|\Psi_2\rangle = 0$ leads to $\tan^2\theta\tan\varphi = -4/\sqrt{15}$. These results for the mixing angles are consistent with the observed Dy magnetic moment and the finding adds credence to our minimal model of Dy properties.

VIII. CONCLUSION

X-ray diffraction data gathered at reflections forbidden in the room temperature crystal structure demonstrates that the structural phase transition at $T_{\mathrm{Q}} = 24.7$ K can be modeled by a change to $P4_2/mnm$ from $P4/mbm$ and a reduction in the Dy site symmetry to $2/m$ from $4/m$. The distorted structure can support an ordered array of time-even Dy multipoles that transform according to the A_g representation of $2/m$. Specifically, the Dy quadrupoles $\langle Q_{\alpha\beta}\rangle$ that order are $\langle Q_{xy}\rangle$ and $\langle Q_{xx} - Q_{yy}\rangle$ where the Cartesian axes x and y lie in the plane normal to the crystal c axis and the axis of two-fold rotation symmetry in $2/m$.

Direct evidence of the spatial ordering of Dy $4f$ quadrupole and hexadecapole moments in DyB_2C_2 is shown by a detailed analysis of the data of azimuthal angle scans measured at two resonant energies ($E1$ and $E2$ resonance) at the Dy L_{III} absorption edge.

Information obtained in electric dipole ($E1$) and electric quadrupole ($E2$) channels of scattering at the Dy L_{III} absorption edge can be combined with specific-heat data, inelastic neutron scattering data on Dy crystal-potential energy levels, and the established magnetic structure that develops below T_{C}

The synthesis of the data is an immediately plausible model of the Dy low-energy states, in which Q_{xy} and the magnetic moment operator behave at successive phase transitions like Ising spin $\frac{1}{2}$ variables. In the model, magnetic moments lie in the $x - y$ plane. The calculated saturation magnetic moment and canting angle are consistent with observations.

[1] M. Arama and P. Morin, J. Phys.: Condens. Matter **10**, 9875 (1998).

[2] M. Arama, R.M. Galéra, P. Morin, and J.F. Bérar, J. Phys.: Condens. Matter **10**, L743 (1998).

[3] H. Adachi, H. Kawata, M. Mizumaki, T. Akao, M. Sato, N. Ikeda, Y. Tanaka, and H. Miwa, Phys. Rev. Lett. **89**, 206401 (2002).

[4] Y. Tanaka, T. Inami, T. Nakamura, H. Yamauchi, H. Onodera, K. Ohoyama, and Y. Yamaguchi, J. Phys.: Condens. Matter **11**, L505 (1999).

[5] D.H. Templeton and L.K. Templeton, Acta Crystallogr., Sect. A: Found. Crystallogr. **41**, 133 (1985).

[6] Y. Murakami *et al.*, Phys. Rev. Lett. **80**, 1932 (1998); **81**, 582 (1998).

[7] M. Benfatto, Y. Joly, and C.R. Natoli, Phys. Rev. Lett. **83**, 636 (1999).

[8] I.S. Elfimov, V.I. Anisimov, and G.A. Sawatzky, Phys. Rev. Lett. **82**, 4264 (1999).

[9] M. Takahashi, J. Igarashi, and P. Fulde, J. Phys. Soc. Jpn. **68**, 2530 (1999); **69**, 1614 (2000).

[10] S. Ishihara and S. Maekawa, Phys. Rev. Lett. **80**, 3799 (1998); Phys. Rev. B **58**, 13442 (1998).

[11] K. Hirota, N. Oumi, T. Matsumura, H. Nakao, Y. Wakabayashi, Y. Murakami, and Y. Endoh, Phys. Rev. Lett. **84**, 2706 (2000).

[12] H. Yamauchi, H. Onodera, K. Ohoyama, T. Onimaru, M. Kosaka, M. Ohashi, and Y. Yamaguchi, J. Phys. Soc. Jpn. **68**, 2057 (1999).

[13] T. Matsumura, N. Oumi, K. Hirota, H. Nakao, Y. Murakami, Y. Wakabayashi, T. Arima, S. Ishihara, and Y. Endoh, Phys. Rev. B **65**, 094420 (2002).

[14] S.W. Lovesey, J. Phys.: Condens. Matter **14**, 4415 (2002).

[15] J.F. Nye, *Physical Properties of Crystals* (Oxford University Press, Oxford, 1985).

[16] J. Igarashi and M. Takahashi, Phys. Rev. B **63**, 184430 (2001).

[17] W. Neubeck, C. Vettier, F. de Bergevin, F. Yakhou, D. Mannix, O. Bengone, M. Alouani, and A. Barbier, Phys. Rev. B **63**, 134430 (2001).

[18] S.W. Lovesey and K.S. Knight, Phys. Rev. B **64**, 094401 (2001).

[19] A. Stunault *et al.*, J. Synchrotron Radiat. **5**, 1010 (1998).

[20] The unit vectors of the polarization of the diffracted beam are

represented by σ' and π', perpendicular and parallel, respectively, to the scattering plane, which includes the wave vector $\mathbf{q}$ of the incident beam and the wave vector $\mathbf{q}'$ of the diffracted beam.

[21] Y. Tanaka *et al.*, J. Phys.: Condens. Matter **15**, L185 (2003).

[22] J. Igarashi and T. Nagao, J. Phys. Soc. Jpn. **72**, 1279 (2003).

[23] T. Nakamura, U. Staub, Y. Narumi, K. Katsumata, and F. Juranyi, Europhys. Lett. **62**, 251 (2003).

[24] S.W. Lovesey, O. Fritz, and E. Balcar, J. Phys.: Condens. Matter **10**, 501 (1998).